Effect of relative humidity on crack propagation in barrier films for flexible electronics

Vellinga, W. P.; De Hosson, J. Th. M.; Bouten, P. C. P.

Published in:
Journal of Applied Physics

DOI:
10.1063/1.4759441

Publication date:
2012

Effect of relative humidity on crack propagation in barrier films for flexible electronics

W. P. Vellinga,[1,a)] J. Th. M. De Hosson,[1] and P. C. P. Bouten[2]
[1]*Materials Innovation Institute, M2i, Department of Applied Physics, University of Groningen, Nijenborgh 4, 9747 AG Groningen, The Netherlands*
[2]*Philips Research Laboratories, High Tech Campus 4, 5656 AE Eindhoven, The Netherlands*

(Received 29 June 2012; accepted 25 September 2012; published online 23 October 2012)

A set of propagating cracks in a SiN barrier film on poly ethylene naphthalate (PEN) were subjected to differing levels of relative humidity. It was observed that the propagation speed of the cracks increased for increasing levels of relative humidity. This was shown using two independent, simultaneous techniques. One of the techniques (a resistance measurement) gives a qualitative measure of the averaged crack tip speed and the other (a microscopic technique) a quantitative measure. An attempt is made to quantify the resistance measurements in terms of crack tip speed. The effects that humidity may have on the crack driving force through differences in hygroscopic expansion are discussed, using independent determination of the diffusion constant of water into PEN. It is concluded that hygroscopic expansion alone cannot account for the observations. © *2012 American Institute of Physics*. [http://dx.doi.org/10.1063/1.4759441]

I. INTRODUCTION

The integrity of thin brittle barrier films is crucial for the proper functioning of flexible electronic devices, such as solar cells, displays, and especially organic light emitting diodes (OLEDs). Such thin brittle layers act as environmental barriers and protect functional layers from interaction with humidity. During processing, various types of inhomogeneities may be incorporated in the films that may lead to stress concentrations when the devices are mechanically loaded. During their lifetime, such devices are subjected to mechanical loads that depend on processing conditions, temperature, humidity, and intended use and that vary with time. Of critical importance is the mechanical stability of the population of pinholes in the barrier films. Pinholes allow diffusion of H_2O through the film and may act as initiation sites for cracking.

Whether existing flaws in a thin film grow depends in a complicated way on its cohesive properties, its thickness, the internal stress state, adhesion to the substrate, and on its defect properties. (for reviews exploring these issues, see, e.g., Refs. 1–3). Moreover, the integrity depends on the interaction with the elastic[4,5] and viscoelastic[6] properties of the substrate and on the chemical interaction with the environment.[7]

Our interest lies in measuring the subcritical crack growth speed in SiN barrier films supported by poly ethylene naphthalate (PEN), and its dependence on the factors mentioned above, specifically the relative humidity (RH). The effects of RH on these stacks have so far received little attention. A change in the RH of the surroundings of a barrier film may act on an existing crack by (1) hygroscopic dimension changes that lead to a change in the crack driving force (energy release rate), (2) changes in the fracture toughness, or (3) changes in the reaction rate

(1) The magnitude of the effect will depend on the difference in the coefficients of hygroscopic expansion α_{RH}^{PEN} and α_{RH}^{SiN}. As a consequence of the difference in hygroscopic expansion, the barrier film is compressed or elongated and elastic energy is stored in it. This changes the amount of energy released on cracking and effectively introduces an RH dependence in the energy release rate G, so $G = G(RH)$ as a consequence of diffusion of water into the materials.
(2) If the surface energy γ of the crack faces is a function of the humidity, $\gamma = \gamma(RH)$ this will have an impact on the fracture toughness.
(3) Assuming a chemical reaction involving H_2O drives subcritical crack propagation, the reaction rate depends on the partial pressure of H_2O (or the RH) and the order n of the reaction.

In the study, we focus on early stages of crack growth during uniaxial tensile deformation and combine optical and electrical methods (e.g., Refs. 8 and 9). The electrical method (a.k.a. "electrofragmentation"[10,11]) measures a resistance R and recently[9] a simple model was proposed which relates this quantity to the crack length and speed in a homogeneously strained sample.

Experimentally observed effects of RH on crack tip speed are presented and discussed, exploring the impact on the energy release rate due to the diffusion of water. As a basis for that discussion, we use an independent determination of the diffusion of water in PEN. The crack tip speed is measured indirectly using a resistance measurement and directly using optical microscopy. A secondary aim of the paper is to check the validity of a simple model description of the dependence of the resistance on the average crack length.

II. EXPERIMENT

The samples used in this paper were similar to the samples described in Ref. 9, which we refer to for more details. Non-stoichiometric PECVD SiN (also containing H) with a thickness of 150 nm was deposited by low temperature

a)Electronic mail: w.p.vellinga@rug.nl.

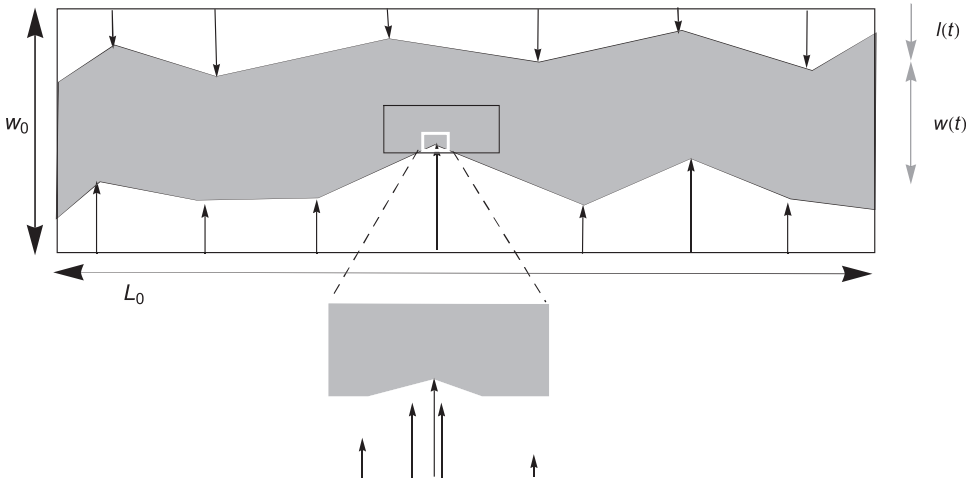

FIG. 1. Sketch of experimental geometry and pattern of propagating cracks. Top: The experimental geometry and a sketch of the subpopulation of cracks that restricts the flow of current. Black arrows indicate cracks and their growth direction. The gray area indicates the area where current is flowing during the resistance measurement. The black rectangle indicates the opening for light transmission. The white rectangle indicates the field-of-view during the experiment ($\approx 0.6 \times 0.5\,\mathrm{mm}^2$). Bottom: An enlargement of the field-of-view of the microscopic experiment, showing a realistic crack density. The crack pattern shown is assumed as a basis for a simplified model description to understand relation between crack length and measured resistance R.

deposition techniques on sheets of poly-ethylene-naphthalate (PEN) with a thickness of 0.125 (mm). Conductive indium-tin-oxide (ITO) with a nominal thickness of 10 nm was deposited on top of the SiN leading to ITO-SiN-PEN samples. In Ref. 9, it was argued that such ITO-SiN films are expected to show essentially the same fracture behaviour as 150 nm SiN films, and in the following the ITO-SiN bilayer is simply referred to as SiN.

Samples were subjected to changes in RH for two different types of loading constraints: clamped as cantilevers for curvature measurements and clamped in a tensile stage in which the crack propagation was measured.

In the curvature measurements (used to estimate the diffusion constant $D^{PEN}_{H_2O}$ of H_2O in PEN), strips of about $80 \times 10 \times 0.125\,\mathrm{mm}^3$ were used. The strips were clamped with their planar dimension vertical in a transparent box that was kept at constant humidity by the presence of a saturated salt. The strips were imaged from the top with a simple digital camera. High contrast was achieved using a black background and by illuminating the strips from the side, the parallel to the SiN-PEN interface normal. In this way, the PEN serves as a light guide and the edges of the strip show high brightness. Points belonging to the cantilevers were isolated from the background using image processing techniques. The curvature was measured by performing a least squares fit of a circle through all the points.

For the tensile experiment, strips of typically $40 \times 7 \times 0.125\,\mathrm{mm}^3$ were used. In the tensile experiments, the samples were mechanically loaded in tension in a Linkam TST-350E tensile stage with temperature, force, and humidity control. The stage allows for investigation with transmission optical microscopy (through an opening of $5.5 \times 1.5\,\mathrm{mm}^2$) and an electronic feed-through makes simultaneous resistance measurements possible.

A. Resistance measurement

For homogeneous loading (i.e., tensile loading, 4-point bending, free bending), we assume that two sets of cracks initiate at damage along the edges of the sample and propagate inwards in a symmetric fashion, as shown in Figure 1.

As long as the two sets of cracks do not interpenetrate, it is possible to define an effective crack length $l(t)$ and an effective width of the remaining conductive channel $w(t) = w_0 - 2l(t)$ (here w_0 is the initial width of the conducting path on the sample) that together determine the resistance $R(t)$. It can be shown (using, for example, finite element calculations) that current is restricted to this conducting path if the distance $d(t)$ between the cracks is much smaller than their length $l(t)$. For the effective length $L(t)$ of the conducting path, we can take $L(t) = L_0$ (since the strains used are small) and it follows that:

$$\frac{R(t)}{R_0} \propto \frac{w_0}{w(t)}, \tag{1}$$

where R_0 is the resistance corresponding to w_0. Using this relation, and keeping in mind that $R(t)/R_0$ should be small, it is possible in principle to relate the change in the relative resistance to the speed of the fastest cracks moving across the sample

$$\frac{d}{dt}\frac{R(t)}{R_0} \propto \frac{w_0}{w^2(t)}\frac{dl(t)}{dt}\left(= \frac{w_0}{(w_0 - 2l(t))^2}\frac{dl(t)}{dt}\right). \tag{2}$$

For very small changes in $l(t)$, $\frac{w_0}{w^2(t)}$ is constant and one finds that the crack tip speed is proportional to $\frac{d}{dt}\frac{R(t)}{R_0}$:

$$\frac{d}{dt}\frac{R(t)}{R_0} \propto \frac{dl(t)}{dt}. \tag{3}$$

In reality, the crack pattern may differ from the pattern shown in Figure 1 since cracks may also originate from positions away from the edge and grow on both crack tips. In that case, it is not *a priori* clear whether Eq. (1) can describe the relation between R and crack movement The appropriateness and the usefullness of Eq. (1) will be discussed in this paper.

B. Microscopy

In contrast to most of the literature, the focus in this paper is on the propagation of subcritical channel cracks and

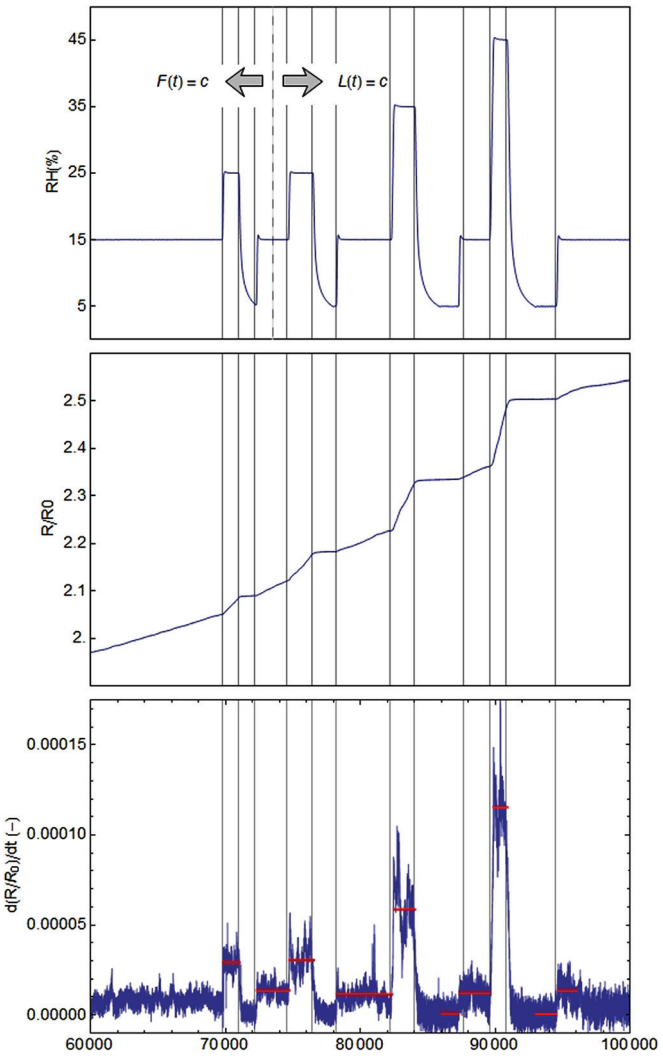

FIG. 2. RH (top), $\frac{R(t)}{R_0}$ (centre), and $\frac{d}{dt}\frac{R(t)}{R_0}$ (bottom) as a function of time. RH was increased from the base value of 15% to 25%, 35%, and 45%, reduced to 5% after each of those steps and brought back to 15%. The thin gray lines indicate positions of steps in RH, they are repeated in some of the following figures as guides to the eye. The dashed line indicates the switch between constant force and constant displacement. Note that the peaks in RH are reproduced as slope changes in $\frac{R(t)}{R_0}$ and as peaks in $\frac{d}{dt}\frac{R(t)}{R_0}$. The straight horizontal lines in $\frac{d}{dt}\frac{R(t)}{R_0}$ are derived from piecewise linear fits to $\frac{R(t)}{R_0}$ in regions where RH was constant.

not on the linear density of cracks (i.e., N/L_0 with N the number of cracks). We have performed simultaneous *in-situ* microscopy to obtain independent quantitative information on the crack growth speeds, and to verify the assumptions of the simple model description discussed in Sec. II A. Transmission bright field microscopy was used to image the crack pattern at various stages during the loading. Digital images were obtained with a Mikrotron CMOS camera with 1280×1024 pixels, operating at 11 Hz. After each grabbed frame N_f frames were discarded, and the effective frame rate was therefore $\frac{11}{N_f+1}$ (1/s). In the experiment N_f was 499, the time between subsequent frames was 45.37 (s). In the experiment discussed in detail here, a time series of around 3000 frames (so, stretching for about 1.4×10^5s) was obtained. Several image processing steps were performed to remove the background due to dust and phase contrast inherent to the sample, a typical example of a raw and a treated image are shown in Fig. 3. The pixel size on the CMOS detector (12 μm) combined with the 25× objective leads to an effective pixelsize of 0.48 μm at the sample, neglecting the slight defocus. The Rayleigh resolution of the objective (NA = 0.4) is about 0.6 μm, meaning that we are slightly oversampling. In this imaging mode, a slight defocus shows the cracks (that have an actual width that is below the Rayleigh resolution of the objective, about 100 nm as observed in SEM) due to phase contrast.[12] The phase contrast is caused by the difference in optical path lengths for paths passing through a crack (PEN only) and paths passing close to a crack (ITO-SiN-PEN). A setting was chosen where the cracks show dark against a light background.

III. RESULTS

A. Relation between $R(t)/R_0$ and RH

In a number of experiments, we have observed consistently that the rate of change of $R(t)/R_0$ depends sensitively on the RH. The example shown in Figure 2 and treated here in detail is typical. Figure 2 shows a prescribed RH together with the response in $\frac{d}{dt}\frac{R(t)}{R_0}$.

In this experiment, a time series of around 3000 frames (stretching for about 1.4×10^5s) was obtained. The RH was set and controlled at 15%, excluding transients after step changes in RH. No independent calibration of RH was undertaken, we assume an error of ±2%. The RH value chosen was close to particularly low values in the lab during a period of severe cold. The temperature was set at 30 °C, somewhat above the lab temperature. The sample was carefully stretched in small steps to the point where $R(t)/R_0 = 1.05$. At this point, no cracks were visible in the field-of-view, or in the entire region available for viewing in the tensile stage which is limited by an elongated hole in the

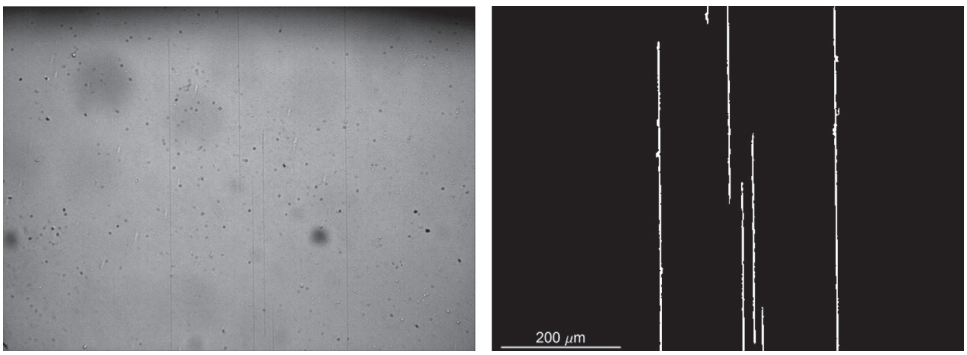

FIG. 3. Example of a raw and a processed image. The raw image shows various types of inhomogeneities with about the same or more contrast than the cracks. Some of the inhomogeneities are due to the imaging (dust) and some to the material. These have not been studied in any detail. In the processed image, it is clear that 7 crack tips are active at this particular moment. The rightmost crack spans the whole field of view and no longer gives information on the crack speed at this time.

heating block. The sample was brought under constant force control (at 32 N) and creep of the substrate led to slow increase in $R(t)/R_0$. At $R(t)/R_0 \approx 1.4$, a crack was identified. At this time, the image acquisition was set up and started. Between $t_{start} = 70000(\mathrm{s})$ $(R(t)/R_0 \approx 2)$ and $t_{end} = 95\ 000(\mathrm{s})$, the RH was changed in steps. Figure 2 shows $\frac{d}{dt}\frac{R(t)}{R_0}$ and RH as a function of time between t_{start} and t_{end}. It should be noted that at time $t_{dis} = 73\,500(\mathrm{s})$ (indicated with the dashed vertical line), the experiment was switched to displacement control. The main reason for this was that the force control system is not completely robust in cases where quick changes occur in RH or T. Because of the appreciable time that had passed since the start of the experiment negligible stress relaxation was expected. In fact, between t_{dis} and t_{end} the force dropped by 0.4 N, about 1.5%–2% of the initial value.

From the various representations in Fig. 2, it is clear that changes in $\frac{d}{dt}\frac{R(t)}{R_0}$ are correlated with changes in RH. It is concluded that $\frac{d}{dt}\frac{R(t)}{R_0}$ and therefore the crack tip speed $v(t)$ increases with increasing RH. This is the main observation in this paper and it is the basis for the discussion in the following.

IV. DISCUSSION

The discussion consists of two parts. First, we want to check the indirect evidence from the resistance measurement and make sure that differences in crack movement indeed underlie the dependence on RH, and not, for example, changes in the resistivity. The microscopic measurements are used here. Second, we want to discuss the causes of the increased speed, focusing on the driving force for cracking, i.e., the role of diffusion of water into PEN and the associated expansion.

A. Microscopic crack propagation measurements

As a check on the validity of the assumptions illustrated in Figure 1 and used in Eqs. (1) and (2), we have performed microscopic measurements of moving cracks simultaneously with the changes in RH illustrated in Figure 2. Considering the potentially wide range of timescales characterising the experiment, it was deemed impractical to obtain data on the propagation of 1 crack and instead we obtained a number of (partly overlapping) time series of the propagation of 9 cracks tips moving across a fixed field-of-view The field-of-view measured approximately 0.6×0.5 mm, which covers $\approx 1/70$th part of the length and $\approx 1/1000$th part of the area of the sample. Figure 3 shows an example of a raw and a processed image, in which 7 active crack tips are visible.

The movement of all crack tips across the field-of-view is illustrated in Figure 4.

The lefthand side of Fig. 4 shows, with colour codes, the progression of the crack tips across the field-of-view. This representation is relevant to the question whether the crack tips are far enough apart to move independently. The smallest distance between two cracks was about 15 μm. This is 100 times the thickness (150 nm) of the SiN film, and based on Ref. 5, we assume that all the cracks were moving independently, i.e., without interaction between the stress fields surrounding their tips. Interaction might lead to changes in crack path or in crack speed when the crack tips approach closely. From the representation in the left hand side of Fig. 4, no changes in crack path are apparent. It is noted that

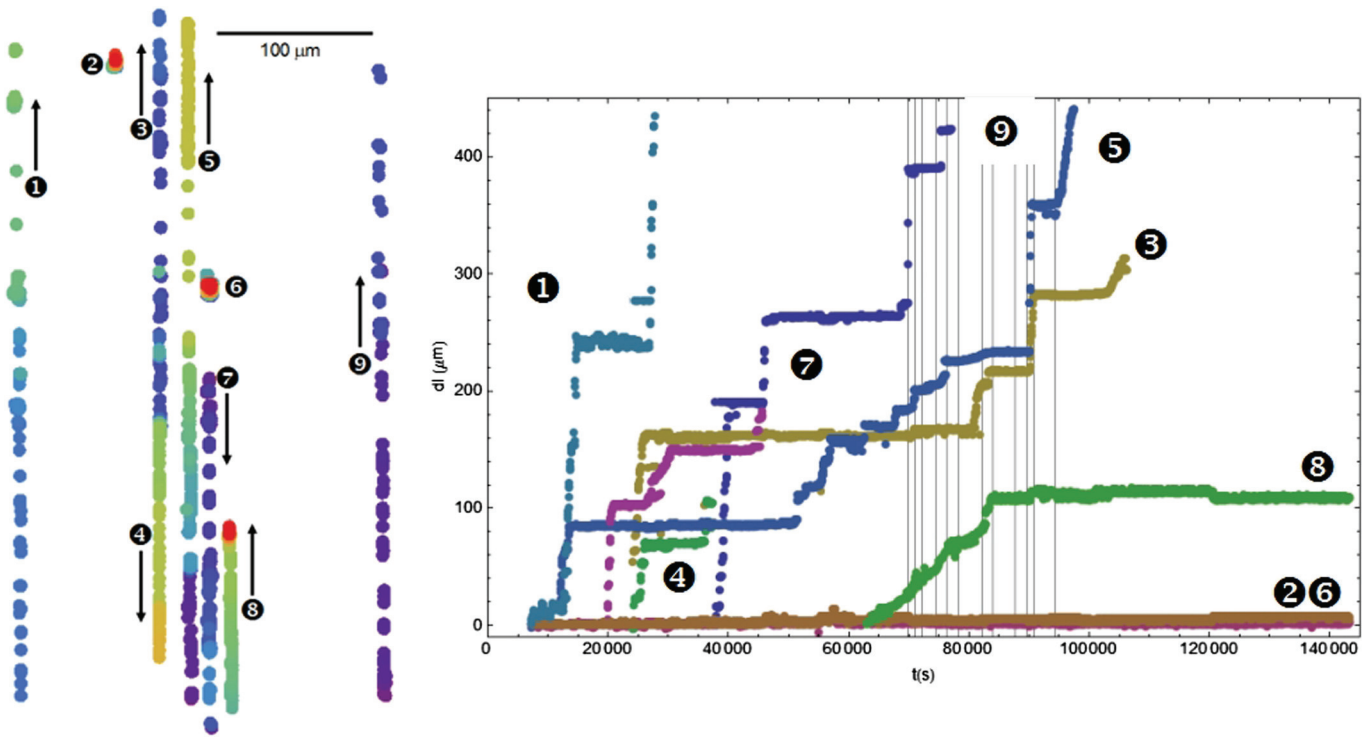

FIG. 4. Left: all measured crack tip positions. Colour indicates moments in time, with purple early and red late times. Right: crack tip displacements as a function of time. Numbers in graphs identify individual crack tips.

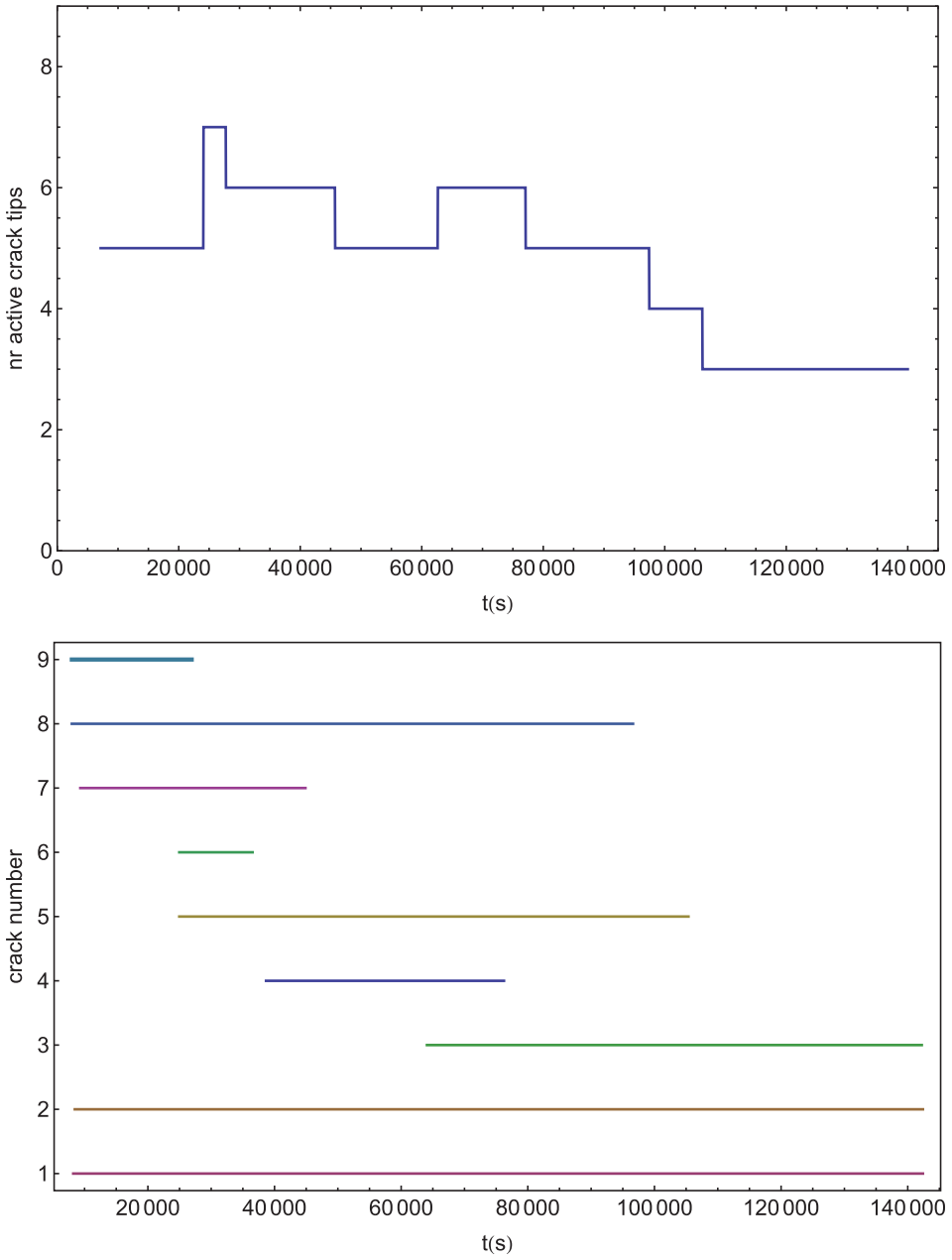

FIG. 5. Number of active crack tips and interval of activity of individual crack tips versus time.

crack tips 2, 6, and 8 remain in the same position for a long time but that they do so starting from a time when no other crack tip is close. It is concluded that the experiments do not show obvious signs of crack interaction. The figure is also relevant in assessing the appropriateness of the simple crack propagation model shown in Figure 1. It is observed that 2 active cracks (crack tips 3, 4 and 6, 7) originate in this field-of-view, in contrast with the sketch in 1.

The righthand side of Fig. 4 shows the absolute values of the displacements inside the field-of-view for 9 crack tips that were visible during the experiment. All lines therefore start at $dl = 0$ and end whenever the crack tip leaves the field-of-view. It is clear from the step-like appearance of the individual graphs during periods of constant RH that the crack speed is not constant, the tips move intermittently. It is noted that the intermittent behaviour of the cracks is similar in the constant force and constant displacement regime. Since the clamps are in no way actuated in the constant displacement regime, the irregularities in the crack movement are thought to originate in the sample itself, possibly to inhomogeneities.

Finally, it is clear that the movement as a function of time for individual crack tips differs significantly and that the relation between the measurements in the righthand side of Figure 4 and those in Figure 2 is not immediately obvious. To relate these observed characteristics of the crack tip movement to $\frac{R(t)}{R_0}$, we start with the average crack movement observed in the field-of-view at time t. This is calculated from

$$\langle dl(t) \rangle = \frac{\sum_{i=1}^{N(t)} dl(t)}{N(t)}, \tag{4}$$

which is the sum of all steps $dl(t)$ at time t divided by the number of active crack tips $N(t)$ (crack tips in the field-of-view) at time t (shown in Figure 5).

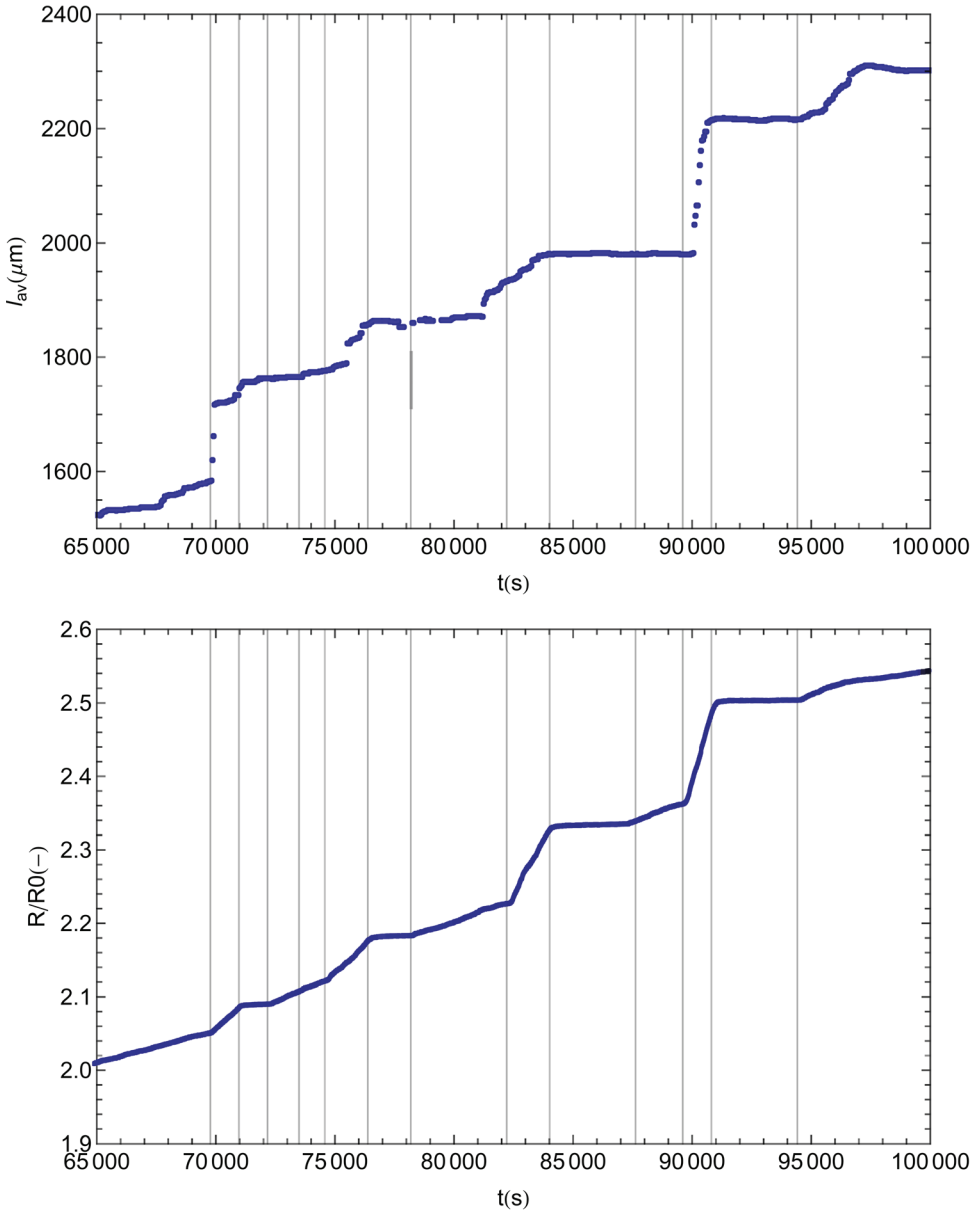

FIG. 6. l_{av} and $R(t)/R_0$ as a function of time.

Using this result we calculate an average crack displacement l_{av}

$$l_{av} = \sum_{all\ frames} \langle dl(t) \rangle. \tag{5}$$

The result that is shown in Figure 6 shows a comparison between l_{av} and $R(t)/R_0$. Piecewise linear fits to the l_{av} data will give values for the observed crack tip speeds v_{obs} at various RH levels.

Figure 6 indicates a correlation between between l_{av} and $R(t)/R_0$. However, the relation between l_{av} and l as used in Eqs. (1) and (2) is not immediately obvious. The task is to relate l_{av} to the position of the current-limiting crack tips, meaning that part of the crack population that moves the fastest. Another approach is to assume that the model shown in Figure 1 can be used in an *effective* sense (i.e., even though the crack pattern observed differs from the one assumed in the model) and to fit $R(t)/R_0$ from Eq. (1) using a simple function $f(l_{eff}) = l_0 + cl_{av}$ that relates the experimentally determined l_{av} to an effective l_{eff}. The two free parameters loosely represent an initial position l_0 and a multiplication factor c that relates the averaged displacement of the crack tip population in the field-of-view to that of the population that restricts the current flow. Using an initial position of $l_0 = 1(\text{mm})$ and $c = 3.3$ a good fit can be obtained see Figure 7.

Using the fit shown in 7 in Eq. (2), we can calculate effective crack tip speeds v_{eff} of the current-limiting cracks based directly on the measurement of $R(t)/R_0$.

Figure 8 shows values for v_{eff} and v_{obs} as a function of RH. In anticipation of the discussion logarithmic axes have been drawn. The main conclusion that is drawn from this figure is that both methods of establishing the crack speed show that the crack tip speed is an increasing function of the RH.

B. Hygroscopic properties of PEN

Since relatively little has been published on the hygroscopic properties of PEN, we performed a few measurements to determine these. In these measurements (used for different

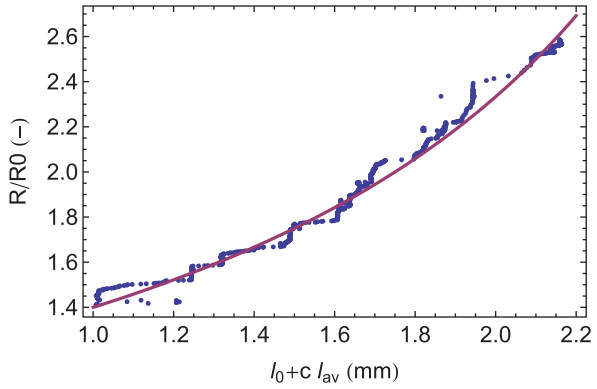

FIG. 7. R/R_0 vs. l_{eff}. Drawn line: expected result according to Eq. (1) taking into account sample dimensions. Dots: experimental results, replacing l_{av} by l_{eff}.

purposes in Ref. 9), a strip of material was clamped on one side and exposed to changing humidity, switching between two saturated salt solutions. The humidity was measured and the curvature was determined from fits of circle segments to photographs of the bent strip. An example of a measurement is shown in Figure 9.

After a step change in the humidity, the curvature changes relatively quickly until it reaches an extremum. Subsequently, it evolves slowly (over the course of days rather than hours) to an equilibrium state in which the curvature is determined by the difference in α_{RH} of SiN and PEN. The existence of such an extremum has been predicted[13,14] and was actually measured on thick metallized PMMA.[15,16] The effect is clearly much larger in the case of the SiN/PEN laminates, but somehow it was not mentioned in Ref. 17.

The graphs of curvature versus time and force versus time were fit using a number of results available in the literature. In Ref. 18, it was found that Henry's law is valid for water in PEN, i.e., there is a linear relation between the partial water of pressure and the water concentration in PEN. Furthermore, it is assumed[18] that that the specific volume of PEN is linearly related to the water concentration.

Using these results and assumptions, a diffusion profile $C(x, t)$ of water in the PEN substrate can be calculated using

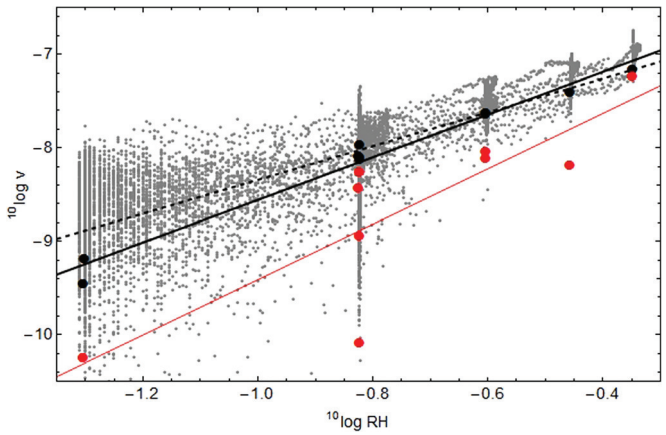

FIG. 8. Values for v_{eff} (large black dots and small grey dots) and v_{obs} (large red dots) as a function of RH. Large dots: Values derived from averages for the periods with constant RH indicated in Figure 2. Small dots: Values derived directly from Figure 2(c).

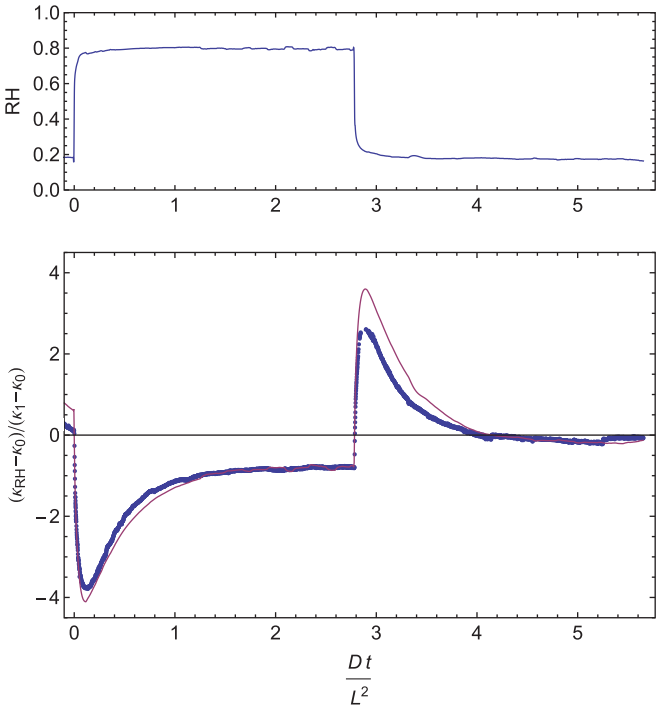

FIG. 9. Top: applied RH. Bottom: measured normalised curvature (dots) and fit (drawn) using diffusion constant $D = 7 \times 10^{-14}(\mathrm{m/s^2})$.

the prescribed RH as input, using finite difference calculations (e.g., Refs. 13 or 14), or numerically integrating an equation given in Ref. 19. Using Refs. 13 or 14, the first moment of $C(x, t)$ can be related to the bending moment. Assuming that the bending moment is linearly proportional to the curvature, the measured values of curvature can be compared to appropriately normalised calculated moments using only the diffusion constant D as a free variable.

The calculations capture the qualitative behaviour very well, see Figure 9 but the value of D used in the fit ($D = 7 \times 10^{-14}(\mathrm{m/s^2})$) is considered to be a rough estimate of the actual value, since the fit is clearly not very good for higher curvatures. An error may be estimated at $\pm 10\%$.

From the same measurements, we also derive an estimate of α_{RH}^{PEN} using the difference in equilibrium curvature between high and low RH situations. For the difference in stress $\Delta\sigma^{hy,SiN}$ between situations with different RH one finds, e.g., Ref. 17

$$\Delta\sigma^{hy,SiN} = \frac{1}{E_{SiN}(1-\nu_{SiN})}\int_{RH_{low}}^{RH_{high}} \left[\alpha_{RH}^{PEN} - \alpha_{RH}^{SiN}\right] dRH. \quad (6)$$

So, assuming that $\alpha_{RH}^{SiN} \ll \alpha_{RH}^{PEN}$ the stress difference can be related to α_{RH}^{PEN} alone. (This assumption seems reasonable but there is little supporting evidence in the literature.[17]) Using a formula proposed by Timoshenko,[20] it is possible to determine the stress in the SiN film, provided that the Young's moduli and Poisson's ratios of substrate and thin film are known

$$\kappa(\epsilon_{hy}) = \frac{6\epsilon_{hy}\left(\frac{h_f}{h_s}+1\right)^2}{(h_c+h_s)\left(3\left(\frac{h_f}{h_s}+1\right)^2 + \left(\frac{\bar{E}_f h_f}{\bar{E}_s h_s}+1\right)\left(\frac{h_f^2}{h_s^2}+\frac{\bar{E}_s h_s}{\bar{E}_f h_f}\right)\right)}. \quad (7)$$

Here, $\bar{E}_i = \frac{E_i}{1-\nu_i}$ with E_i the Young's modulus, ν_i the Poisson's ratio, and $i = f$ or $i = s$. In practice, measurement of the Young's moduli of thin hard films supported by polymers is difficult. For ITO values of 88.4±11.3 GPa (Brillouin light scattering),[21] 92 GPa (Vickers indentation),[21] 99.8±13.6,[22] 112 GPa (nanoindentation on ITO coatings deposited on glass substrates),[2] 116 GPa,[23] and 118 GPa[24] have been reported. For the systems discussed here, with a low substrate modulus, the displacements that occur can be rather large even though the strains remain small. In this case, solutions based on non-linear elasticity are appropriate as was shown by Ref. 25. Solutions for rectangular strips were shown to be in accordance with experiment in, e.g., Ref. 26. We will use the expressions given in these papers to relate measured curvature to stresses in the SiN assuming that the ITO has the same modulus as the SiN so that the system effectively consists of 2 layers. This assumption may be too strong since for PECVD SiN film density, hydrogen content, internal stress, and elastic properties are correlated, as shown by Ref. 27.

For the difference in the stress (using the same measurements as in Ref. 9), we find significantly different values for a film with high internal stress and a film with low internal stress: 200 MPa and 110 MPa. Yet another film with high internal stress gave 165 MPa. Since the PEN films were the same, this would seem to indicate that there is a difference in the properties of the types of SiN used. That this may be the case has been argued in Ref. 27. Ignoring this, we find an average for the stress of 160 ± 45 MPa. Further using 133 GPa as effective modulus, we find $\alpha_{RH}^{PEN} \approx 22$ (ppm/RH). Values in the literature (e.g., Refs. 28 and 29) and from manufacturers data sheets are usually smaller ranging from 7 to 15 ppm. Clearly, ours is not a very precise method of determining α_{RH}^{PEN} but in the following we will only need the order of magnitude of the value determined.

C. Effect of RH on crack propagation

In the introduction, we stated that a change in the RH may act on an existing crack by hygroscopic dimension changes that lead to a change in the crack driving force (the energy release rate G), by changes in the fracture toughness γ or by changes in the reaction rate at the crack tip. These effects appear in the following formula for crack speed $v(RH)$ (compare, e.g., Ref. 30):

$$v(RH) \sim c_0 RH^n \exp\left(\frac{G(RH) - 2\gamma(RH)}{2NkT}\right). \quad (8)$$

Here c_0 is a constant, N is the number of bonds per unit cracked area, k is Boltzmann's constant, and T is the absolute temperature. The energy release rate G(RH) is described by

$$G = Z\frac{\pi}{2}\frac{h_f\sigma^2}{\bar{E}_f} = Z\frac{\pi}{2}h_f\epsilon^2\bar{E}_f. \quad (9)$$

The constant Z depends on the elastic mismatch between film and substrate and on the geometry, and can be expressed as a function of the Dundurs parameters. The effect of elastic mismatch on G has been calculated by Beuth[4] for a film on a half space and Vlassak[31] showed that for systems of stiff films on compliant substrates with $h_s/h_f > 1000$ the solution of Beuth is essentially correct. The occurrence of the strain term in Eq. (9) directly explains the effect of the hygroscopic strain.

In an extreme case, changing the RH from 0% to 100% and allowing the sample to reach equilibrium, which would take in the order of a day, induces a hygroscopic strain of the PEN of 0.05%-0.2%. The lower estimate is based on literature values for α_{RH}^{PEN} and the higher estimate on the value determined in Sec. IV B).

The 0.2% dimension change in this extreme case would certainly be significant considering that typical breaking strains are in the order of 0.8% (e.g., Ref. 9). Samples equilibrated at the extreme levels used in this experiment, i.e., 15-10% RH and 15 + 30% RH would show compressive strains between −0.005% and −0.02% or tensile strains between 0.015% and 0.06%, respectively. These values must be considered maxima for the contributions due to RH in this experiment. In practice, the contributions are thought to be *much* smaller due to (1) the relatively rapid cycling of the RH and (2) the mechanical constraints on the sample in the experiment.

ad (1). For the experiment described, we calculated diffusion profiles of water in PEN as a function of time and determined the spatial average concentration as a function of time (see Fig. 10). We find that there is a maximum average concentration equivalent to RH = 17.5% (or 15% + 2.5%) and a minimum average concentration equivalent to RH = 14.0% (or 15%–1%). ad (2). For a PEN sample *free to expand*, the maximum strain difference caused by these excursions (+2.5% and −1%) is expected to be only around 0.007%, or 1/100th of the breaking strain. The experiment was performed in constant displacement and an effect on the clamping force was observed that was roughly in accordance with this. However, due to the same constraint, the actual strain difference of the SiN is expected to remain much smaller than 0.007%. We think it is safe to say that the observed difference in crack speed is not associated with the expansion caused by the average change in water content of the sample.

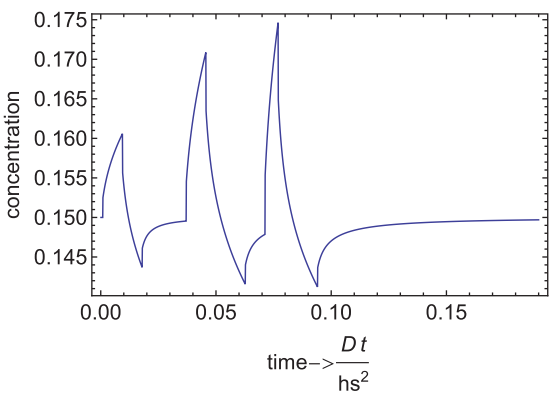

FIG. 10. Calculated average concentration of water in PEN as a function of time during the experiment, in units of equivalent equilibrium RH value.

The previous line of reasoning centered on replacing the actual concentration distribution with an average concentration and on homogeneous deformation associated with it. The change in energy release rate due to the change in average H_2O content in the substrate was excluded as the origin of the change in crack speed. But in fact the distribution of water in the sample is not homogeneous. Near the bottom of the substrate and the floor of a crack, the concentration of H_2O in the PEN quickly assumes the equilibrium value, which shows much larger excursions during the experiment than the average value.

The concentration gradient stretching from the bottom of the substrate will tend to cause bending of the sample (as was shown in Ref. 9). However, during the experiment bending is restricted due to the constraints posed by the clamps and by the tensile stress and is believed to be negligible (and certainly none was observed as changes in focus during the microscopy). In any case for RH $>$ 15% or $<$15%, the tendency would be to put the SiN under compression or tension, respectively, i.e., leading to effects *opposite* to those observed.

There is also local diffusion into the bottom of cracks, leading to local strains in the wake of the crack tip. In fact, it is this particular contribution due to diffusion that distinguishes parts of the film far ahead of the crack tip from those far behind the crack tip thereby potentially contributing to the energy release rate. In this case for RH $>$ 15%, the tendency would be toward local expansion of the PEN and an increase in the crack opening much like in a wedge test. However, the energy released must be smaller than in the case discussed above of the homogeneously loaded sample at -10% RH and $+30\%$ RH which would show a compressive strains of -0.005% to -0.02% or tensile strains of 0.015% to 0.06%, respectively. Clearly, the crack opening must be much smaller than in that case, since only a tiny part of the sample (the wake of the crack) has absorbed any water and since expansion is countered by the constraints on the sample.

Considering the above, we conclude that the correlation observed in Figure 2 is not due to hygroscopic dimension changes. The change in crack speed is therefore due to a chemical interaction of the SiN with H_2O. Changes in the RH influence the reaction rate and/or the fracture toughness. For a change in the reaction rate, a power-law relation between RH and crack tip speed is expected. The fits to the three data sets shown in 8 show indications that a power-law behaviour is indeed observed here. The method outlined above may therefore be suitable to study the dependence of the crack speed on RH for a material in a single experiment.

V. CONCLUSIONS

We have observed a clear dependence of the crack speed in SiN barrier films on relative humidity. Cracks were found to propagate faster in high relative humidity surroundings. This was shown by a comparison of resistance measurements to time series of micrographs of propagating cracks. The microscopic measurements show that the cracks move intermittently. Inhomogeneities in the material are thought to be solely responsible since the cracks were too far apart to interact. A method was described to obtain an effective crack displacement from data on a series of moving crack tips across a fixed field-of-view. It was established that the evolution of the resistance could be linked to this effective crack displacement using a simple model description for the crack pattern and a simple linear relation between the effective crack length in the model and the observed effective crack length. Based on observations on diffusion of H_2O in PEN and resulting values for the diffusion coefficient and the coefficient of hygroscopic expansion, it was concluded that the effect on speed was mainly due to a change in the fracture toughness, i.e., a change in chemical interaction between the SiN and the surroundings. These appear to be the first measurements that combine microscopy and resistance measurements in this way. We conclude that this type of measurement is a useful tool in the study of crack propagation or static fatigue of barrier films on polymer substrates.

ACKNOWLEDGMENTS

This research was carried out under Project No. MC7.07299 in the framework of the Research Program of the Materials innovation institute M2i (www.m2i.nl). Ferdie van Assche of TNO/Holst Centre, the Netherlands, is thanked for preparation of the ITO-SiN-PEN material.

[1]Y. Leterrier, "Durability of nanosized oxygen-barrier coatings on polymers," Prog. Mater. Sci. **48**, 1–55 (2003).
[2]P. C. P. Bouten, R. J. Slikkerveer, and Y. Leterrier, "Mechanics of ITO on plastic substrates for flexible displays," in *Flexible Flat Panel Displays*, edited by G. P. Crawford (John Wiley & Sons, Ltd., 2005), Chap. 6, pp. 99–120.
[3]J. Lewis, "Material challenge for flexible organic devices," Mater. Today **9**, 38–45 (2006).
[4]J. Beuth, Jr., "Cracking of thin bonded films in residual tension," Int. J. Solids Struct. **29**, 1657–1675 (1992).
[5]J. Ambrico, "The role of initial flaw size, elastic compliance and plasticity in channel cracking of thin films," Thin Solid Films **419**, 144–153 (2002).
[6]Z. Suo, J. Prévost, and J. Liang, "Kinetics of crack initiation and growth in organic-containing integrated structures," J. Mech. Phys. Solids **51**, 2169–2190 (2003).
[7]J. Vlassak, Y. Lin, and T. Tsui, "Fracture of organosilicate glass thin films: Environmental effects," Mater. Sci. Eng., A **391**, 159–174 (2005).
[8]D. R. Cairns, R. P. W. Ii, D. K. Sparacin, S. M. Sachsman, D. C. Paine, and G. P. Crawford, "On polymer substrates," Appl. Phys. Lett. **76**, 1425–1427 (2000).
[9]W. P. Vellinga, J. T. M. De Hosson, and P. C. P. Bouten, "Direct measurement of intrinsic critical strain and internal strain in barrier films," J. Appl. Phys. **110**, 044907 (2011).
[10]A. Pinyol, B. Meylan, D. Gillieron, V. Mewani, Y. Leterrier, and J. Manson, "Electro-fragmentation analysis of dielectric thin films on flexible polymer substrates," Thin Solid Films **517**, 2000–2006 (2009).
[11]Y. Leterrier, A. Pinyol, L. Rougier, J. H. Waller, and J.-A. E. Manson, "Electrofragmentation modeling of conductive coatings on polymer substrates," J. Appl. Phys. **106**, 113508 (2009).
[12]U. Agero, L. G. Mesquita, B. R. A. Neves, R. T. Gazzinelli, and O. N. Mesquita, "Defocusing microscopy," Microsc. Res. Tech. **65**, 159–165 (2004).
[13]F.-Z. Xuan, S.-S. Shao, Z. Wang, and S.-T. Tu, "Influence of residual stress on diffusion-induced bending in bilayered microcantilever sensors," Thin Solid Films **518**, 4345–4350 (2010).
[14]F. Yang and J. C. M. Li, "Diffusion-induced beam bending in hydrogen sensors," J. Appl. Phys. **93**, 9304–9309 (2003).
[15]F. Bruder and W. H. Aese, "Water absorption and transient tilt of polymeric substrates for optical data storage media γ," Jpn. J. Appl. Phys. **38**, 1709–1710 (1999).

[16]L. V. D. Tempel, "Deformation of polycarbonate optical discs by water sorption and aging," in *Precision Injection Molding*, edited by J. Greene and R. Wimberger-Friedl (Hanser, Munich, 2006), Chap. 7, pp. 153–168.
[17]P. Dumont, G. Tornare, Y. Leterrier, and J. Manson, "Intrinsic, thermal and hygroscopic residual stresses in thin gas-barrier films on polymer substrates," Thin Solid Films **515**, 7437–7441 (2007).
[18]H. Zhang and I. M. Ward, "Kinetics of hydrolytic degradation of poly (ethylene naphthalene-2, 6-dicarboxylate)," Macromolecules **28**, 7622–7629 (1995).
[19]L. C. Evans, *Partial Differential Equations* (American Mathematical Society, 1998).
[20]S. Timoshenko, "Analysis of bi-metal thermostats," J. Opt. Soc. Am. **11**, 233–255 (1925).
[21]T. Wittkowski, "Elastic properties of indium tin oxide films," Thin Solid Films **398–399**, 465–470 (2001).
[22]K. Zeng, "Investigation of mechanical properties of transparent conducting oxide thin films," Thin Solid Films **443**, 60–65 (2003).
[23]D. Neerinck and T. J. Vink, "Depth profiling of thin ITO films by grazing incidence X-ray diffraction," Thin Solid Films **278**, 12–17 (1996).
[24]J.-I. Han, *Stability of Externally Deformed ITO Films* (John Wiley & Sons, Ltd., 2005), Chap. 7, pp. 121–134.
[25]C. Masters and N. Salamon, "Geometrically nonlinear stress-deflection relations for thin film/substrate systems," Int. J. Eng. Sci. **31**, 915–925 (1993).
[26]M. D. Tran, W. P. Vellinga, and J. H. Dautzenberg, "Curvature of rectangular coated foils with different width-to-length ratios," Mater. Res. Soc. Symp. Ser. **505**, 533–538 (1998).
[27]S. King, R. Chu, G. Xu, and J. Huening, "Intrinsic stress effect on fracture toughness of plasma enhanced chemical vapor deposited SiNx:H films," Thin Solid Films **518**, 4898–4907 (2010).
[28]D. V. D. Berg, M. Barink, P. Giesen, E. Meinders, and I. Yakimets, "Hygroscopic and thermal micro deformations of plastic substrates for flexible electronics using digital image correlation," Polym. Test. **30**, 188–194 (2011).
[29]M. Barink, M. Goorhuis, P. Giesen, F. Furthner, and I. Yakimets, "Prediction of the thermo-mechanical material behavior of PEN foil during photolithographic processing," EuroSimE 2009-10th International Conference on Thermal, Mechanical and Multi-Physics Simulation and Experiments in Microelectronics and Microsystems, 2009, pp. 1–4.
[30]S.-Y. Kook and R. H. Dauskardt, "Moisture-assisted subcritical debonding of a polymer/metal interface," J. Appl. Phys. **91**, 1293 (2002).
[31]J. J. Vlassak, "Channel cracking in thin films on substrates of finite thickness," Int. J. Fract. **119**, 299–312 (2003).